Single-molecule super-resolution imaging of T-cell plasma membrane CD4 redistribution upon HIV-1 binding

Yue Yuan[1 *], Caron Jacobs[1,2,3 *], Isabel Llorente Garcia[4 *], Pedro M. Pereira[1,5], Scott P.Lawrence[1], Romain F. Laine[1,6 ✉], Mark Marsh[1 ✉], and Ricardo Henriques[1,6,7 ✉]

[1]MRC Laboratory for Molecular Cell Biology, University College London, London, UK
[2]SAMRC/NHLS/UCT Molecular Mycobacteriology Research Unit, Department of Pathology, Institute of In-fectious Disease and Molecular Medicine, University of Cape Town, Cape Town, South Africa
[3]Wellcome Centre for Infectious Diseases Research in Africa, University of Cape Town, Cape Town, South Africa
[4]Department of Physics and Astronomy, University College London, London, UK
[5]Bacterial Cell Biology, MOSTMICRO, Instituto de Tecnologia Química e Biológica António Xavier, Univer-sidade Nova de Lisboa, Oeiras, Portugal
[6]The Francis Crick Institute, London, UK
[7]Instituto Gulbenkian de Ciência, Oeiras, Portugal
[*]Equal contributing authors

The first step of cellular entry for the human immunodeficiency virus type-1 (HIV-1) occurs through the binding of its envelope protein (Env) with the plasma membrane receptor CD4 and co-receptor CCR5 or CXCR4 on susceptible cells, primarily CD4$^+$ T cells and macrophages. Although there is considerable knowledge of the molecular interactions between Env and host cell receptors that lead to successful fusion, the precise way in which HIV-1 receptors redistribute to sites of virus binding at the nanoscale remains unknown. Here, we quantitatively examine changes in the nanoscale organisation of CD4 on the surface of CD4$^+$ T cells following HIV-1 binding. Using single-molecule super-resolution imaging, we show that CD4 molecules are distributed mostly as either individual molecules or small clusters of up to 4 molecules. Following virus binding, we observe a local 3-to-10-fold increase in cluster diameter and molecule number for virus-associated CD4 clusters. Moreover, a similar but smaller magnitude reorganisation of CD4 was also observed with recombinant gp120. For the first time, our results quantify the nanoscale CD4 reorganisation triggered by HIV-1 on host cells. Our quantitative approach provides a robust methodology for characterising the nanoscale organisation of plasma membrane receptors in general with the potential to link spatial organisation to function.

HIV-1 entry | viral receptor | nanoscale cluster | super-resolution microscopy | CD4 | STORM | quantitative analysis | modelling

Correspondence:
r.laine@ucl.ac.uk, m.marsh@ucl.ac.uk and rjhenriques@igc.gulbenkian.pt

Introduction

Cell surface receptor binding is a key step in cell infection by viruses, initiating processes that allow viral particles to cross the plasma membrane and deliver their genetic material to the host cell (1). To infect CD4$^+$ T cells, and other immune cells such as macrophages, the human immunodeficiency virus type-1 (hereafter referred to as HIV) requires binding to the surface glycoprotein CD4, and either CCR5 or CXCR4 (depending on strain tropism) as co-receptors. Biochemical and structural studies have led to a well-developed biomechanical model of the conformational changes in the viral envelope glycoprotein (Env) triggered by receptor/co-receptor binding, that lead to the formation of a fusion pore between the plasma membrane and the viral envelope. However, understanding of how receptor molecules are recruited to cell surface-bound virus particles is currently limited (2).

Previous work has suggested that receptor clustering is crucial for many receptor-ligand signalling interactions (3). For example, on T cells, T-cell receptors (TCRs) have been shown to coalesce into nanoclusters within and around immune synapses before signal transduction (4–6). Viral protein and cell-surface receptor organisation may also play a role in the local recruitment of molecules needed for successful HIV entry (7–9). Because the Env subunit gp120-CD4 single inter-molecular bonds are short-lived (~0.24 s lifetime) (10) compared to the typical duration of virus entry (in the order of minutes from receptor binding to fusion), multiple Env-CD4 interactions and CD4 receptor clustering are likely to be required for HIV entry (2). In terms of the virus itself, previous studies have established that Env trimers redistribute and cluster on the surface of virions following Gag cleavage and maturation (11). Given that the number of Env trimers per HIV virion is low (approx.10 (12–14)), this clustering facilitates the formation of multiple receptor interactions for virus entry. Although the number of Env trimers required for virus entry is currently controversial (2), there may be a minimal local requirement for Env proteins on HIV particles and receptors on the target cell membrane for successful virus binding and fusion.

Little is known about how HIV receptor organisation on the target cell surface may facilitate, or be modulated by, virus binding. To date, most of the evidence for redistribution and clustering of cell-surface CD4 and co-receptors to sites of virus binding comes from confocal immunofluorescence

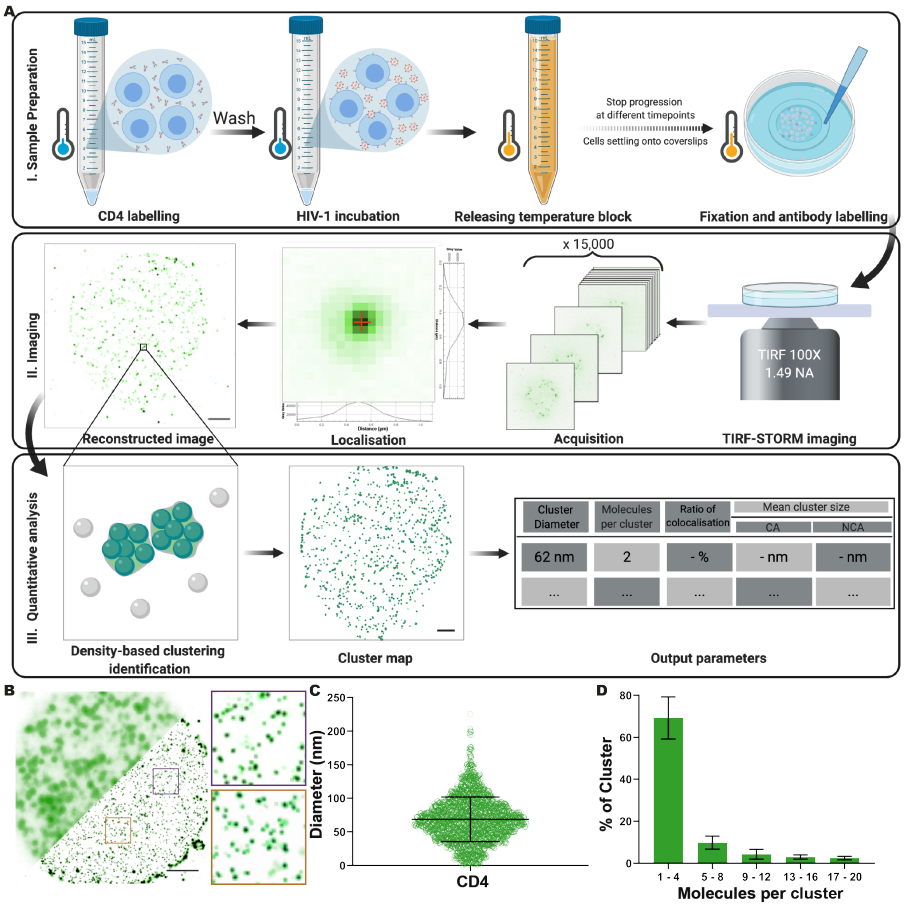

Fig. 1. Experimental and analytical pipeline for the quantitative analysis of plasma membrane CD4. A. Schematics of the experimental and analytical pipelines used. (I) SupT1-R5 cells were pre-incubated at 4℃ with OKT4 with or without HIV or gp120, prior to a brief release of the temperature block and rapid chemical fixation. (II) Cells deposited on imaging surfaces were imaged using a standard TIRF-STORM acquisition, and (III) localisations were used for density-based cluster analysis and molecular counting. **B.** Representative diffraction-limited TIRF (top half) and TIRF-STORM (bottom half) images of CD4 in an untreated SupT1-R5 cell. Insets show enlarged TIRF-STORM images of the indicated regions. Scale bar = 2 µm. **C.** Quantification of CD4 cluster diameters in the same cells. Each point represents 1 cluster; 15 cells were measured, giving a total of 11768 clusters. Bars represent mean ± SD. **D.** Molecular counting of CD4 clusters. Each bar represents the percentage of clusters displaying the indicated ranges of molecules per cluster. Bars represent mean ± SD. All data represent at least three independent experiments.

microscopy studies with spatial resolution limited to ~200-300 nm (more than 20 times the size of individual receptor molecules) (7, 15–19). Super-resolution microscopy can study cellular organisation at the scale of an infecting viral particle (~120 nm) (20). In particular, single-molecule localisation microscopy (SMLM) techniques such as stochastic optical reconstruction microscopy (STORM) (21) allow individual cell-surface proteins to be mapped on intact cells (5, 22–24). Moreover, coordinate maps of all detected localisations can be analysed using point pattern methods, such as DBSCAN (density-based spatial clustering of applications with noise) (25), allowing the quantification of single-molecular nanoscale information. SMLM not only allows us to understand single molecule assemblies, but also provides information on potential interaction by protein colocalisation analysis, such as coordinate-based colocalisation analysis (CBC) (26). Clus-DoC (27), an SMLM data analysis platform, which unifies DBSCAN and CBC for cluster detection and colocalisation, facilitates implementation of these analytical approaches and has previously been used to examine T-cell signalling by characterising the geometric relationships between phosphorylated and non-phosphorylated TCR (28).

In addition to distribution analysis, SMLM data can be used to count the number of fluorescently labelled molecules in a dataset, as demonstrated by estimations of the number of CD4 molecules per cluster in untreated T cells (4), TCRs upon cell activation (24), and glutamate receptors in presynaptic zones (29). It has also recently been used to estimate the number of Influenza A virus (IAV) receptors, and to characterise their reorganisation during virus binding (30). In the latter study, the authors established a pipeline to count the approximate number of molecules per cluster from STORM data and discovered that co-clustering between receptor sialic acid and epidermal growth factor receptor serves as an initial platform for IAV binding and signalling (30).

Although three recent super-resolution microscopy studies have reported CD4 cluster sizes in the range ~100-350 nm on resting T cells (4, 31, 32), here we used STORM imaging and a robust analytical pipeline to characterise the membrane distribution of CD4 at the single-molecule, nanoscale level and show that HIV binding induces rapid localised clustering of CD4 on $CD4^+$ T cells. Using this imaging-based approach, we measured a 3-to-10-fold increase in the diameter of HIV-associated CD4 clusters, and an increased number of CD4 molecules per cluster (13-16 molecules, compared to 1-4 molecules in the absence of HIV). We further explored the reorganisation of CD4 clusters with statistical modelling: Cluster-size specific Poisson statistics were used to model the distributions of CD4 molecules. We found that the receptor-number distribution in HIV-bound cells differs from that predicted by a random distribution of receptors. Together, these approaches provide a novel view of the initial events of HIV binding and entry and indicate a link between a functional role and the spatial organisation of cell-surface receptors. The imaging and analytical pipeline we set out here

can be used to explore the nanoscale distribution and function of other cell-surface receptors, opening the way to new insights into the molecular events underlying signal transduction.

Results

Analysis of CD4 nanoclusters on CD4⁺ T cells by quantitative super-resolution imaging.

In order to study the effect of HIV-binding on the organisation of CD4 molecules at the cell surface, we first established an experimental and analytical framework to quantitatively characterise nanoscale receptor organisation (Fig.1). To avoid potential artefacts caused by fixation and antibody-induced artificial crosslinking, we developed an experimental assay in which immunolabeling and receptor-virus binding were carried out at low temperature to minimise membrane fluidity and trafficking (33–35). Although HIV-target cell-binding occurs at 37°C *in vivo*, virus bound at 4°C can display CD4-specific association and occupy an intermediary state in the cell entry process referred to as a temperature arrested state (TAS) (33–35). A subsequent brief release of the temperature block and rapid cell fixation allowed us to capture receptor reorganisation at early stages following virus binding (Fig.1AI). We have previously carefully evaluated cell fixation protocols to preserve native membrane protein organisation (36), and we confirmed that antibody binding did not lead to detectable artificial crosslinking or perturbation of receptor distribution on the time scales of our assays (Fig.S1).

We used TIRF-STORM to image CD4 in the cell membrane adjacent to the glass (Fig.1AII), followed by Clus-Doc (27) to identify clusters and estimate their shape parameters (area, equivalent diameter and localisation density; Fig.1AIII). The diameter results produced by Clus-Doc (27) were validated by comparison with manual cluster annotation, confirming the suitability of this approach (Fig.S2). TIRF-STORM imaging and cluster characterisation in untreated SupT1-R5 cells revealed CD4 is arranged in small clusters of 64 nm ± 33 nm diameter (Fig.1B and C), with the majority (aprox.70%) composed of 1 to 4 CD4 molecules (Fig.1D).

To determine if our analysis pipeline could robustly identify changes in CD4 organisation, we used chemical induction to redistribute CD4 in a predictable and controllable manner. Treatment with the phorbol ester PMA stimulates clathrin-mediated endocytosis (CME) of CD4 by activation of a phosphorylation-dependent dileucine signal (37). SupT1-R5 cells were treated with PMA for 15 minutes, as previously described (38), and imaged with TIRF-STORM. Quantification of CD4 localisations revealed the formation of large plasma membrane CD4 clusters (93 nm ± 36 nm diameter; Fig.2A, B). At the single cluster level, a clear pool of larger CD4 clusters of up to 800 nm diameter was seen (Fig.2C). Increased cluster diameters were not detected in cells fixed im-

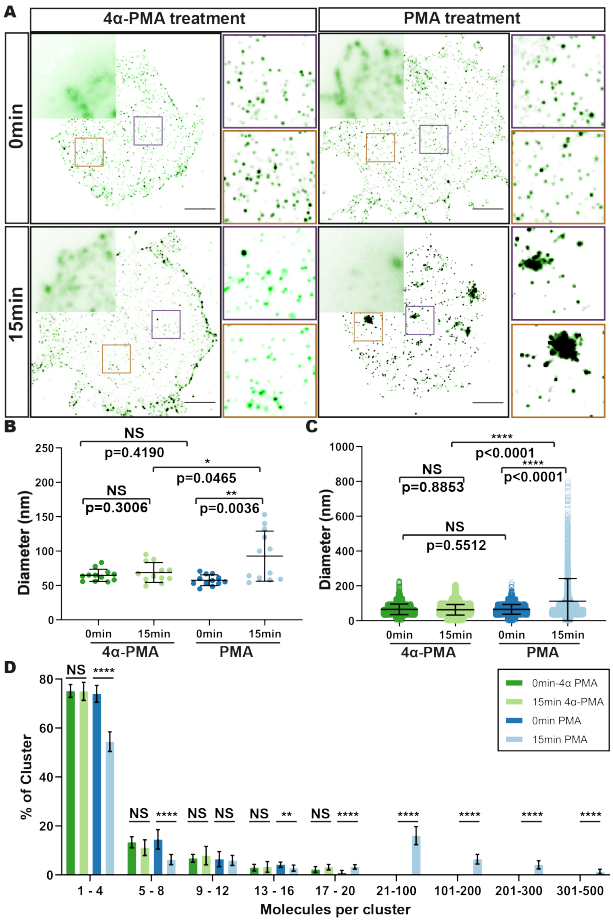

Fig. 2. CD4 reorganisation in response to PMA and 4α-PMA.A. Representative TIRF (top left corner) and TIRF-STORM (bottom) images of CD4 clusters in SupT1-R5 cells following treatment for 0 minutes (top) or 15 minutes (bottom) with 4α-PMA (left) or PMA (right). Insets show magnified TIRF-STORM images of the indicated regions. Scale bar = 2 µm. **B. and C.** Quantification of CD4 cluster diameters; (B) each dot represents the average cluster diameter per cell and (C) each dot represents the diameter of individual clusters. 15 cells were measured per condition; bars indicate the mean ± SD. **D.** Molecule counting of CD4 clusters. Each bar represents the mean cluster fraction displaying the indicated ranges of molecules per cluster. Data are representative of at least three independent experiments. Bars represent mean ± SD. * p< 0.05; ** p< 0.01; *** p< 0.001; **** p< 0.0001.

mediately following PMA addition, nor in those treated with non-stimulatory 4α-PMA (Fig.2B, C), both of which showed cluster diameter distributions similar to that of untreated cells (as in Fig.1C). Localisation-based estimates indicated that PMA induced an increase in the number of CD4 molecules per cluster (21 - 100 molecules per cluster; average of 38 ± 73) and, strikingly, a small number of clusters with as many as 500 molecules (Fig.2D). This CD4 reorganisation is an expected consequence of PMA treatment and indicates that our pipeline should detect potential HIV-induced changes in the cell-surface CD4 distribution.

HIV receptor binding induces changes in CD4 clustering.

Although HIV cell entry is dependent on the initial binding of CD4 molecules by the viral Env subunit gp120, how receptor binding impacts on the nanoscale organisation of CD4 is

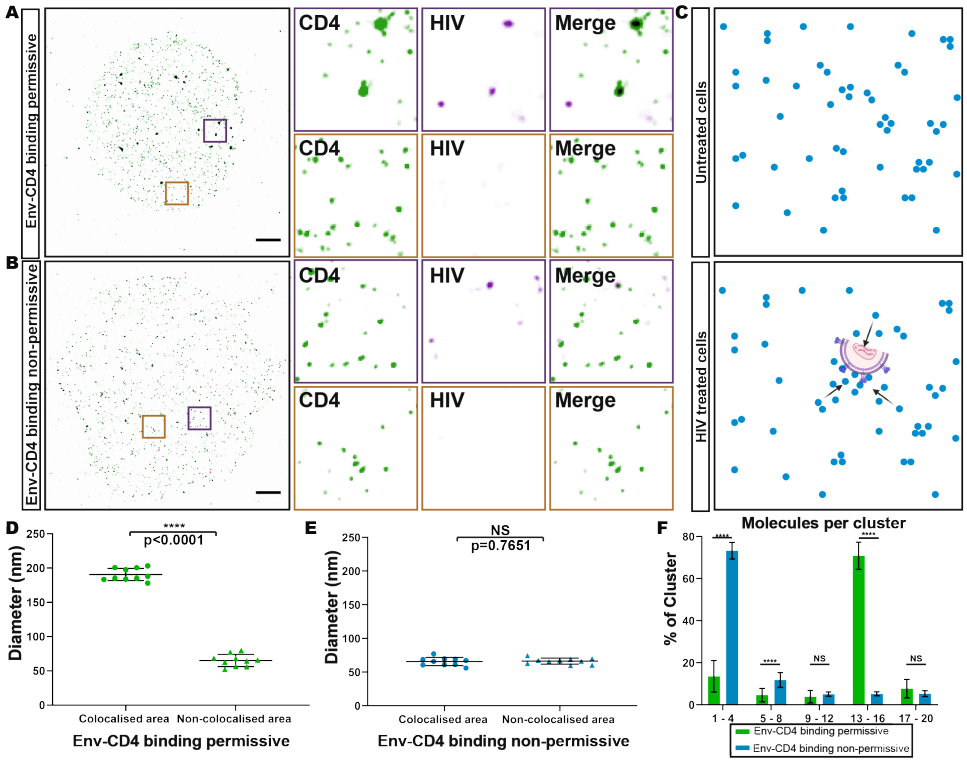

Fig. 3. Analysis of HIV-bound CD4 clusters.A. and B. Representative TIRF-STORM images, and selected magnified regions (insets), of cell-surface CD4 (green) and HIV-1 p24 (magenta). Scale bar = 2 µm. **C.** Schematic of cell-surface CD4 molecules (blue) in untreated cells (upper panel) and HIV treated cells (lower panel). **D. and E.** Quantification of CD4 cluster diameters in the absence (D) or presence (E) of Q4120. Each dot represents the average CD4 cluster diameter on one cell. 10 cells were measured per condition, bars indicate mean ± SD. The data are representative of at least three independent experiments. **F.** Molecule counting of colocalised areas in the absence (Env-CD4 binding permissive) or presence of Q4120 (Env-CD4 binding non-permissive). Bars indicate mean ± SD. * p< 0.05; ** p< 0.01; *** p< 0.001; **** p< 0.0001.

poorly understood (2). Therefore, we set out to measure the effect of virus binding on CD4 nanoscale organisation using our quantitative pipeline.

We incubated SupT1-R5 cells with HIV_{JR-CSF} under CD4-binding permissive (Fig.3A) or non-permissive (Fig.3B) conditions (i.e. in the presence of the neutralizing anti-CD4 antibody Q4120 inhibits Env-CD4 binding [46]), followed by brief treatment at 37°C before rapid fixation. Dual-colour TIRF-STORM imaging of immunolabeled CD4 and HIV p24 (Fig.3A, B) revealed enlarged CD4 clusters around HIV contact sites in permissive conditions, but not in non-permissive control conditions (Fig.3D, E). Using coordinate-based colocalisation analysis built into Clus-DoC, we identified and characterised CD4 clusters that were associated with cell-surface bound HIV. HIV-colocalised CD4 clusters were more than twice the diameter of non-HIV-colocalised clusters on the same cells (191 ± 6 nm vs 71 ± 8 nm, respectively; Fig.3D). The diameters of non-associated clusters were in good agreement with those measured on untreated cells (65 ± 9 nm vs 64 ± 33 nm, respectively; Fig.3E). This increase in cluster diameter was not observed when HIV binding was blocked by Q4120 (65 ± 6 nm), nor in HIV-treated cells that were fixed prior to 37°C incubation (63 ± 8 nm) (Fig.3B, E and Fig.S3). In conditions permissive for receptor binding, the increase in CD4 cluster diameter was accompanied by an equivalent increase in the number of CD4 molecules per cluster; 70% of clusters consisted of 13-16 molecules, compared to 1-4 molecules per HIV-associated cluster when receptor binding was inhibited (Fig.3F). These results were further validated by HIV-CD4 colocalisation analysis which showed that around 80% of HIV particles were engaged with CD4 clusters in permissive conditions (Fig.S4). In contrast, less than 5% of viral particles were associated with CD4 clusters in non-permissive conditions in the presence of Q4120 (Fig.S4B). This HIV-associated change in clustering was dependent on incubation at 37°C after release of the TAS (Fig.S3), and the CD4 cluster changes were abrogated by inhibition of HIV-CD4 interactions (Fig.3B, E). These data indicate that HIV-receptor binding at the plasma membrane induced an increase in local CD4 clustering around bound viral particles in a manner dependent on direct interaction between the virus and receptors. Importantly, this reorganisation did not lead to a general increase in the density of CD4 molecules across the fields imaged (Fig.S5A), or within the larger clusters (Fig.S5B), indicating that the increase in cluster diameters is due to local accumulations of CD4 molecules (Fig.3C and Fig.S5).

Next, we compared the changes in CD4 organisation induced by HIV to a theoretical Poisson statistical model used to calculate the distribution of the numbers of molecules per cluster that could be expected from a random distribution of receptors on the cell surface. An overall CD4 surface density (n) of 200 molecules/µm^2 was used, based on the number of CD4 molecules per cell reported for SupT1 cells (39, 40), and the different cluster sizes measured experimentally were used to generate an averaged theoretical Poisson distribution (see Fig.4A and Materials and Methods). In untreated cells, the experimental data was similar to the modelled distribution (Fig.4B). However, in samples with HIV bound under permissive conditions, the experimentally measured data showed a clear additional peak at 13-16 molecules per cluster that cannot be explained by the theoretical random distri-

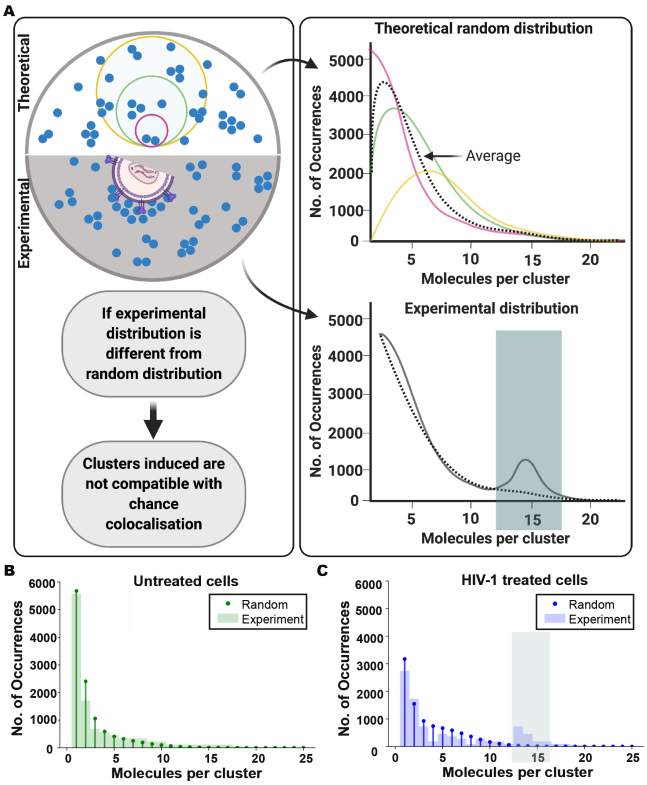

Fig. 4. Statistical modelling of CD4 surface distribution. A. Model schematic (Top): counting CD4 molecules (blue) in membrane areas of different sizes (small (pink), medium (green) or large (yellow)) compared to a theoretical model based on an averaged Poisson distribution that corresponds to a random distribution of receptors on the cell surface and to multiple measurements in membrane areas (clusters) of different sizes (the black line is the average of Poisson distributions for different cluster sizes [pink, green, yellow]). Bottom: Experimentally determined distribution: HIV binding alters the organisation of receptors, the occurrence of clusters of a certain number of molecules per cluster is altered (solid line) and the distribution differs from the expected averaged Poisson distribution (dotted line). **B. and C.** Comparison of modelled ('Random') and measured distributions of the numbers of molecules per cluster for untreated cells (B) and HIV-treated cells (C). The discrepancy between the predicted model and the experimental data in HIV-treated cells is highlighted in green shading in A and C. Data from at least three separate experiments and total 15 different cells in each condition, respectively.

bution model. Specifically, we measured an approximately four-fold increase in the fraction of clusters with 13-16 CD4 molecules when HIV was present (Fig.4C), with that fraction corresponding to an increase in cluster diameters (Fig.S5C). We also tested the effect of possible variations in cell-surface CD4 levels or cell size by generating theoretical Poisson distributions as above, using overall density values of n = 60 molecules/μm^2 and n = 300 molecules/μm^2. When we tested our experimental data against these models, we saw a similar clear additional peak at 13-16 molecules per cluster that was not predicted by the theoretical model (Fig.S6). These results support the notion that the observed CD4 cluster reorganisation is a result of HIV binding.

HIV gp120-induced CD4 clustering is independent of CCR5.

Our data suggest that HIV binding induces a reorganisation of CD4 at the cell surface, promoting local concentrations of CD4 molecules, as indicated by an increase in CD4-cluster diameters and CD4 molecules per cluster. Based on these findings, we posited that the increased CD4 clustering could be a biological requirement for productive HIV binding and/or entry. We sought to explore this hypothesis by assessing the ability of HIV Env to locally recruit CD4 using a reductionist approach. For this purpose, we analysed CD4 organisation following soluble gp120 binding, using a similar approach to that described above for HIV binding. TIRF-STORM imaging and cluster characterisation of CD4 on gp120-treated SupT1-R5 cells revealed increased cluster diameters following the release of the temperature block (84 ± 12 nm) (Fig.5A (left) and B), although to a lesser extent than that induced by intact HIV (191 ± 6 nm) (Fig.3D). This change in cluster diameters was accompanied by a higher variation in CD4 molecules per cluster – a decrease in the number of the smallest clusters of up to 4 molecules, and small increases in the number of clusters consisting of 5-8 and 13-16 molecules (Fig.5C). This indicated that upon binding, gp120 alone can locally influence CD4 distribution, although the extent of this effect was less than that induced by viral particles.

CD4 binding by gp120 in functional Env trimers stabilises an 'open' Env conformation that permits subsequent Env binding to a co-receptor – e.g. CCR5 - which, in turn, drives membrane fusion and viral entry (34, 41). To determine whether the changes observed in cell-surface CD4 organisation following HIV binding were dependent on the presence of the co-receptor, in this case CCR5, we compared CD4 clustering on gp120-bound SupT1-R5 cells to that on SupT1 cells which do not express CCR5. No difference was detected in mean cluster diameter (86 ± 18 nm vs 84 ± 12 nm), or on the number of CD4 molecules per cluster, in the presence or absence of CCR5 (Fig.5A [right] and B). These results suggest that local recruitment of CD4 molecules immediately following gp120 binding is not dependent on the presence of a co-receptor.

Discussion

Knowledge of the initial stages of virus infection i.e., the molecular details under-pinning the interaction between viral proteins and host-cell receptors, is essential for a full understanding of the mechanism through which HIV enters cells. While HIV probably first attaches to cells through diverse interactions with various adhesion factors (42–46), the virus is dependent on binding to CD4 and the co-receptors CCR5 or CXCR4 for successful fusion with the target cell membrane (47). Previous studies have pointed to a role for both Env and CD4 clustering in HIV entry (15–17, 48–51), however, the relationship between the spatial distribution of receptors and the fusion process has remained largely speculative. To understand this process in more detail, we sought to characterise the nanoscale organisation of cell surface HIV receptor proteins during virus binding and entry. Here we describe the use

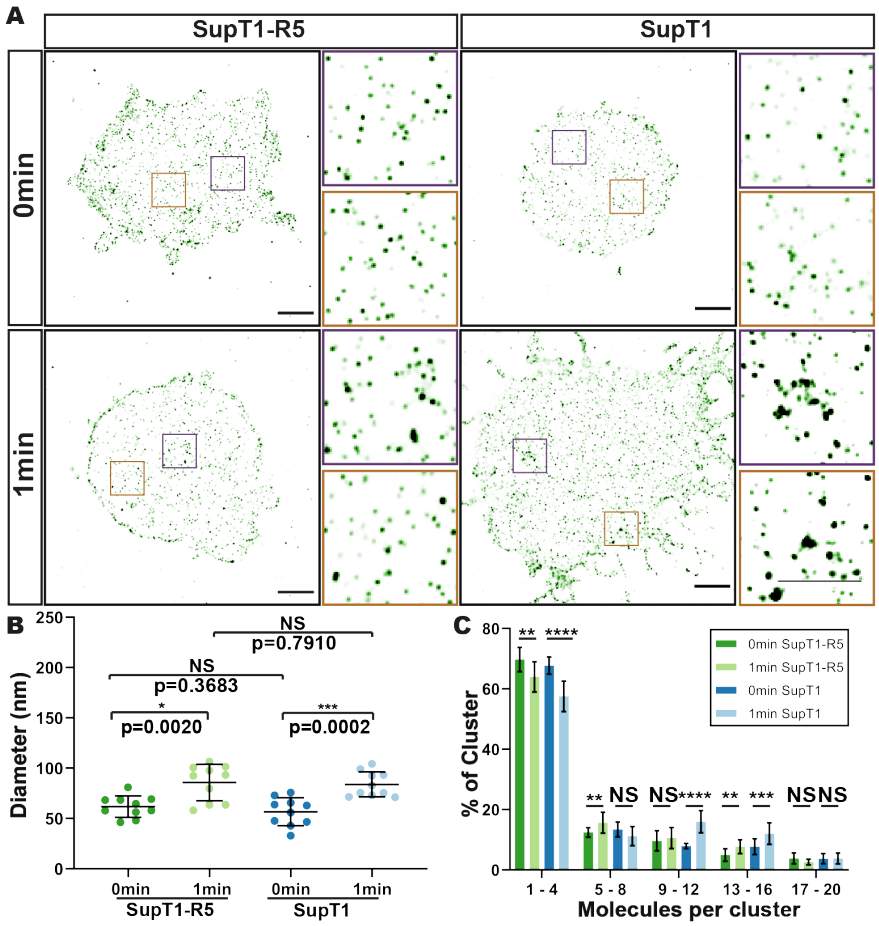

Fig. 5. CD4 nanoscale organisation following binding of gp120 in SupT1-R5 and SupT1 cells.A. Representative TIRF-STORM images of CD4 on SupT1-R5 cells (left) and SupT1 cells (right), fol-lowing gp120 and OKT4-AlexaFluor 647 pre-binding and warming for 1min prior to fixation. Control samples were fixed directly following gp120 treatment. Insets show magnified TIRF-STORM images of the indicated regions. Scale bars = 2 µm. **B.** Mean receptor cluster diameters per cell are plotted for each gp120-treated SupT1 and SupT1-R5 condition. Each point represents the mean value for a single cell. **C.** Molecule counting; the cluster fraction per range of molecule numbers is plotted for each condition. The error bars plot the overall mean and SD. * p< 0.05; ** p< 0.01; *** p< 0.001; **** p< 0.0001.

of super-resolution SMLM and a suite of analytical tools to determine the organisation of CD4 in response to HIV binding.

We established an experimental and analytical pipeline with the necessary range and sensitivity to detect nanoscale receptor organisation. Although SMLM provides significantly improved lateral and axial spatial resolution, most membrane receptor studies are conducted via two-dimensional imaging and neglect cell-surface nanotopography. Immobilisation of cells on a glass surface for imaging in TIRF mode can sometimes interfere with the complex cell-surface morphology. For instance, the flattening of T-cells on PLL-coated glass can cause artefacts when studying membrane receptor (re)organisation (52–54). In our study, we co-incubated HIV and $CD4^+$ T cells in suspension before depositing the cells on PLL-coated coverslips to minimise potential artefacts induced by cell-glass interactions.

To verify that our approach could identify nanoscale changes in CD4 organisation, we tested this pipeline using PMA, a known inducer of CD4 clustering and clathrin-mediated CD4 endocytosis (38) (Fig.1 and 2). Density-based nanoscale analysis of CD4 organisation on untreated T cells revealed that CD4 is distributed into nanoscale domains containing a single molecule or small clusters of up to four CD4 molecules (Fig.1). These results agree with a growing body of evidence that cell-surface receptors are generally organised into clusters (5, 22, 41, 55), some on a scale similar to membrane nanodomains (50-200 nm), that may correspond to the corrals organised by the cortical actin meshwork (56–58). However, the term 'cluster' can be challenging to define in SMLM because detected localisations could represent a single molecule or small group of molecules. We adopted a definition from similar work that studied TCR distributions, specifically that nanoclusters are 'molecules grouped at a sub-diffraction limit scale (< 250nm), such that the grouped coordinates are unlikely to be completely randomly distributed' (59).

Using SMLM localisation, we were able to obtain estimates of the numbers of CD4 molecules per localisation or cluster, following the approach described by Sieben et al (30). Considering that the numbers of molecules counted was mostly <10 per cluster, it is important to note that these figures should be considered as rough estimates and not true numbers of molecules. The accurate determination of molecule numbers using SMLM methods remains a challenge due to labelling efficiency, re-emitting fluorophores, variable imaging conditions and differences in analytical approaches (60). A potential undercounting in our experiments may arise from low labelling efficiency. In particular, we may underestimate the number of CD4 molecules as OKT4, the anti-CD4 antibody used in this work, has a lower binding efficiency compared to, for example, the neutralizing anti-CD4 antibody Q4120. Q4120 is more commonly used for characterising cell-surface CD4 but is unsuitable for HIV-CD4 interaction

studies. Although the CD4 levels per cell measured in this study (total number of molecules/the area of a region of interest) are lower than those reported previously (60 molecules/ μm^2 vs 200 molecules/ μm^2) (39, 40), given the very different measuring techniques used, the numbers are reasonably close. The post-processing calibration for molecule counting implemented here may also lead to undercounting. The process depends on the gap time distribution parameter selected when quantifying the dark time used to calibrate the experimental localisation coordinate lists. The gap time distribution fitting is a trade-off between over-merging (i.e. high confidence but underestimated protein count) and under-merging (i.e. lower confidence but higher protein count). In this study, a longer gap time was used to minimise false-positive molecular identifications. Despite these uncertainties, we can nevertheless extract useful information by emphasising the relative changes in molecule numbers under different experimental conditions. Our results consistently indicate a 3-to-10-fold increase in both cluster diameter and the number of molecules assembled around bound HIV particles (Fig.3).

To further confirm that the CD4 clustering detected on cells with bound HIV was not attributable to chance, we applied statistical modelling to simulate a random distribution of receptors on the cell surface and compared our results with the experimental data (Fig.4). Based on previously reported numbers of ~100,000 CD4 molecules/SupT1 cell (39, 40), and an average T-cell radius of 10 µm, we assumed an overall mean density (n) of 200 CD4 molecules/ μm^2 in our model (Fig.4). To compare this estimate with our experimental data, we estimated the number of CD4 molecules on SupT1-R5 cells labelled with Q4120 and OKT4. We measured a density of 180 molecules/μm^2 with Q4120 and 60 molecules/ μm^2 with OKT4. Given these antibodies recognise different epitopes on the CD4 molecule, we regard these measurements as being in reasonable agreement. Nevertheless, to take possible variations in detected CD4 levels and in cell size into account, we tested our model at lower and higher mean density values of n = 60 molecules/μm^2 and n = 300 molecules/μm^2 (Fig.S6). In all cases, our conclusions stand, i.e. HIV binding induces CD4 clustering, as opposed to clustering being a product of occasional random accumulation. This statistical model allows us to assign greater confidence to our interpretation of the data and the biological significance of receptor clustering changes. Importantly, this framework can be easily adapted to studies of other membrane-associated receptors and induced organisational changes. Given the measured density of CD4 molecules within the HIV-induced clusters (approx.500 molecules/ μm^2), we estimated the intermolecular centre-to-centre distances for CD4 molecules as 40-50 nm. This distance is larger than the measured width of trimeric Env complexes of 10–15 nm (15, 49, 61, 62). Even considering the likely undercounting in our data, this suggests that not all gp120 molecules on an individual Env spike engage CD4. Further, given that mature HIV particles have an average of 10 Env trimers per virion (12–14), which can be arranged in clusters in the viral envelope (11, 50). Our measured numbers of 13-16 CD4 molecules in an HIV-associated cluster suggests an approximate ratio of 1:1 CD4 per Env trimer. Nevertheless, it remains difficult to estimate the precise Env-CD4 stoichiometry required for fusion and entry, as the organisation of the relevant Env-CD4 interactions within each virus-CD4 cluster remains to be established. For membranes to fuse, both CD4 and Env molecules, as well as other proteins, must be cleared from the zone of close approach of the opposing bilayers. Thus, CD4-Env interactions might be organised as a ring at the edge of the cell-virus interface. In part at least, this might underlie the observation that the measured CD4 clusters have diameters that exceed those of virus particles (typically approximately 120 nm) and point to a larger biophysical influence for Env trimer clustering than previously thought, potentially requiring flexibility in Env and/or CD4 as recently shown for the spike (S) protein of SARS-CoV-2 (63).

From a downstream mechanistic point of view, although signalling through the GPCR co-receptors has been identified as a process that HIV can exploit to remodel the cytoskeleton and facilitate productive infection (62), there are conflicted reports as to whether GPCR-dependent signalling through CCR5 is required for HIV entry (64, 65). The CD4 clustering we observed, coupled with the independence of gp120-induced CD4 clustering from co-receptor CCR5, suggests that HIV-induced signalling through CD4 and Lck (such as that detected by Lucera et al (64)) can trigger CD4 clustering beyond the range of Env binding. Furthermore, CD4/Lck signalling, while not essential for HIV infection (macrophages are Lck-negative yet HIV-susceptible), may play a more significant role in facilitating efficient HIV entry in some cell types than previously appreciated.

In summary, our study provides the first nanoscale analysis of HIV-induced spatial changes in cell-surface CD4 distribution during the initial steps of HIV infection. HIV-induced CD4 spatial reorganisation might link to their functional role during HIV binding and fusion. This work contributes to our goal of better understanding how viruses spatially modulate cell-surface receptors to facilitate their entry, and how we might prevent virus infection by inhibiting not only receptor binding but also receptor spatial redistribution. The imaging and analytical pipeline we have established provides a powerful and robust toolbox to further study HIV entry as well as the properties of other virus-receptor systems and membrane proteins in general.

Acknowledgements

We thank James A. Hoxie for providing HEK-293T, SupT1 and SupT1-R5 cell lines. We thank Christian Sieben for sharing the Matlab scripts and helpful discussions on molecule counting. We also thank the MRC LMCB Light Microscopy Facility for support.

Author contribution

Conceptualization, R.H., M.M., R.F.L., I.L.G., Y.Y. P.M.P., S.P.L and C.A.J. ; methodology, R.H., M.M., R.F.L., I.L.G., P.M.P., S.P.L., Y.Y. and C.A.J.; software, Y.Y., R.F.L., I.L.G.; validation, Y.Y., C.A.J., R.F.L.; formal analysis, Y.Y, R.F.L. and I.L.G.; data curation, Y.Y. and C.A.J.; writing,original draft preparation, Y.Y., C.A.J.; writing, review and editing, R.H., M.M., R.F.L., I.L.G., P.M.P., S.P.L., Y.Y. and C.J.; visualization, Y.Y.; supervision, R.H., M.M., R.F.L.; P.M.P and S.P.L. funding acquisition, R.H. and M.M. All authors have read and agreed to the published version of the manuscript.

Funding

M.M. and R.H. were supported by the UK Medical Research Council funding to the MRC-UCL LMCB University Unit (MC_UU00012/1 and MC_U12266B). R.F.L. would like to acknowledge the support of the MRC Skills Development Fellowship (MR/T027924/1). Y.Y. was supported by the Biotechnology and Biological Sciences Research Council (BB/M009513/1) and UCL Overseas Research Scholarship. C.A.J. was a Commonwealth Scholar funded by the UK government and a Wellcome Trust Centre for Infectious Diseases Research in Africa fellowship (the centre is sup-ported by core funding from the Wellcome Trust [203135/Z/16/Z]). This project has received funding from the European Research Council (ERC) under the European Union's Horizon 2020 research and innovation programme (grant agreement No. [101001332]).

Conflicts of Interest

The authors declare no conflict of interest.

EXTENDED AUTHOR INFORMATION

- Yue Yuan: 0000-0002-6698-3009; Julie_YueYuan
- Caron Jacobs: 0000-0002-8072-4433; caron_ajacobs
- Isabel Llorente Garcia: 0000-0002-4282-7714
- Pedro M. Pereira: 0000-0002-1426-9540; MicrobeMatos
- Scott P.Lawrence: 0000-0002-2887-3933
- Romain F. Laine: 0000-0002-2151-4487; LaineBioImaging
- Mark Marsh: 0000-0002-0213-3259; MarkCPMarsh
- Ricardo Henriques: 0000-0002-2043-5234; HenriquesLab

Bibliography

1. Joe Grove and Mark Marsh. The cell biology of receptor-mediated virus entry. *Journal of Cell Biology*, 195(7):1071–1082, 2011.
2. Isabel Llorente García and Mark Marsh. A biophysical perspective on receptor-mediated virus entry with a focus on hiv. *Biochimica et Biophysica Acta (BBA)-Biomembranes*, 1862 (6):183158, 2020.
3. Niña C Hartman and Jay T Groves. Signaling clusters in the cell membrane. *Current opinion in cell biology*, 23(4):370–376, 2011.
4. Kyung-Ho Roh, Björn F Lillemeier, Feng Wang, and Mark M Davis. The coreceptor cd4 is expressed in distinct nanoclusters and does not colocalize with t-cell receptor and active protein tyrosine kinase p56lck. *Proceedings of the National Academy of Sciences*, 112(13): E1604–E1613, 2015.
5. Björn F Lillemeier, Manuel A Mörtelmaier, Martin B Forstner, Johannes B Huppa, Jay T Groves, and Mark M Davis. Tcr and lat are expressed on separate protein islands on t cell membranes and concatenate during activation. *Nature immunology*, 11(1):90–96, 2010.
6. Yair Razvag, Yair Neve-Oz, Julia Sajman, Oren Yakovian, Meital Reches, and Eilon Sherman. T cell activation through isolated tight contacts. *Cell Reports*, 29(11):3506–3521, 2019.
7. Scott P Layne, Michael J Merges, Micah Dembo, John L Spouge, and Peter L Nara. Hiv requires multiple gp120 molecules for cd4-mediated infection. *Nature*, 346(6281):277–279, 1990.
8. Shawn E Kuhmann, Emily J Platt, Susan L Kozak, and David Kabat. Cooperation of multiple ccr5 coreceptors is required for infections by human immunodeficiency virus type 1. *Journal of Virology*, 74(15):7005–7015, 2000.
9. Emily J Platt, James P Durnin, Ujwal Shinde, and David Kabat. An allosteric rheostat in hiv-1 gp120 reduces ccr5 stoichiometry required for membrane fusion and overcomes diverse entry limitations. *Journal of molecular biology*, 374(1):64–79, 2007.
10. Melissa I Chang, Porntula Panorchan, Terrence M Dobrowsky, Yiider Tseng, and Denis Wirtz. Single-molecule analysis of human immunodeficiency virus type 1 gp120-receptor interactions in living cells. *Journal of virology*, 79(23):14748–14755, 2005.
11. Jakub Chojnacki, Dominic Waithe, Pablo Carravilla, Nerea Huarte, Silvia Galiani, Jörg Enderlein, and Christian Eggeling. Envelope glycoprotein mobility on hiv-1 particles depends on the virus maturation state. *Nature communications*, 8(1):1–10, 2017.
12. Ping Zhu, Elena Chertova, Julian Bess, Jeffrey D Lifson, Larry O Arthur, Jun Liu, Kenneth A Taylor, and Kenneth H Roux. Electron tomography analysis of envelope glycoprotein trimers on hiv and simian immunodeficiency virus virions. *Proceedings of the National Academy of Sciences*, 100(26):15812–15817, 2003.
13. Ping Zhu, Jun Liu, Julian Bess, Elena Chertova, Jeffrey D Lifson, Henry Grisé, Gilad A Ofek, Kenneth A Taylor, and Kenneth H Roux. Distribution and three-dimensional structure of aids virus envelope spikes. *Nature*, 441(7095):847–852, 2006.
14. Elena Chertova, Julian W Bess Jr, Bruce J Crise, Raymond C Sowder II, Terra M Schaden, Joanne M Hilburn, James A Hoxie, Raoul E Benveniste, Jeffrey D Lifson, Louis E Henderson, et al. Envelope glycoprotein incorporation, not shedding of surface envelope glycoprotein (gp120/su), is the primary determinant of su content of purified human immunodeficiency virus type 1 and simian immunodeficiency virus. *Journal of virology*, 76(11): 5315–5325, 2002.
15. Sonia Jiménez-Baranda, Concepción Gómez-Moutón, Ana Rojas, Lorena Martínez-Prats, Emilia Mira, Rosa Ana Lacalle, Alfonso Valencia, Dimiter S Dimitrov, Antonella Viola, Rafael Delgado, et al. Filamin-a regulates actin-dependent clustering of hiv receptors. *Nature Cell Biology*, 9(7):838–846, 2007.
16. Sophie Ugolini, Maxime Moulard, Isabelle Mondor, Nicolas Barois, Denis Demandolx, James Hoxie, Anne Brelot, Marc Alizon, Jean Davoust, and Quentin J Sattentau. Hiv-1 gp120 induces an association between cd4 and the chemokine receptor cxcr4. *The Journal of Immunology*, 159(6):3000–3008, 1997.
17. Santos Mañes, Gustavo del Real, Rosa Ana Lacalle, Pilar Lucas, Concepción Gómez-Moutón, Sonsoles Sánchez-Palomino, Rafael Delgado, José Alcamí, Emilia Mira, and Carlos Martínez-A. Membrane raft microdomains mediate lateral assemblies required for hiv-1 infection. *EMBO reports*, 1(2):190–196, 2000.
18. Ling Yi, Jun Fang, Nilgun Isik, Jimmy Chim, and Tian Jin. Hiv gp120-induced interaction between cd4 and ccr5 requires cholesterol-rich microenvironments revealed by live cell fluorescence resonance energy transfer imaging. *Journal of Biological Chemistry*, 281(46): 35446–35453, 2006.
19. Oliver F Brandenberg, Carsten Magnus, Peter Rusert, Roland R Regoes, and Alexandra Trkola. Different infectivity of hiv-1 strains is linked to number of envelope trimers required for entry. *PLoS Pathog*, 11(1):e1004595, 2015.
20. Jakub Chojnacki and Christian Eggeling. Super-resolution fluorescence microscopy studies of human immunodeficiency virus. *Retrovirology*, 15(1):41, 2018.
21. Michael J Rust, Mark Bates, and Xiaowei Zhuang. Sub-diffraction-limit imaging by stochastic optical reconstruction microscopy (storm). *Nature methods*, 3(10):793–796, 2006.
22. Wolfgang WA Schamel and Balbino Alarcón. Organization of the resting tcr in nanoscale oligomers. *Immunological reviews*, 251(1):13–20, 2013.
23. Eilon Sherman, Valarie Barr, and Lawrence E Samelson. Super-resolution characterization of tcr-dependent signaling clusters. *Immunological reviews*, 251(1):21–35, 2013.
24. Benedikt Rossboth, Andreas M Arnold, Haisen Ta, René Platzer, Florian Kellner, Johannes B Huppa, Mario Brameshuber, Florian Baumgart, and Gerhard J Schütz. Tcrs are randomly distributed on the plasma membrane of resting antigen-experienced t cells. *Nature immunology*, 19(8):821–827, 2018.
25. Martin Ester, Hans-Peter Kriegel, Jörg Sander, Xiaowei Xu, et al. A density-based algorithm for discovering clusters in large spatial databases with noise. In *Kdd*, volume 96, pages 226–231, 1996.
26. Sebastian Malkusch, Ulrike Endesfelder, Justine Mondry, Márton Gelléri, Peter J Verveer, and Mike Heilemann. Coordinate-based colocalization analysis of single-molecule localization microscopy data. *Histochemistry and cell biology*, 137(1):1–10, 2012.
27. Sophie V Pageon, Philip R Nicovich, Mahdie Mollazade, Thibault Tabarin, and Katharina Gaus. Clus-doc: a combined cluster detection and colocalization analysis for single-molecule localization microscopy data. *Molecular biology of the cell*, 27(22):3627–3636, 2016.
28. Sophie V Pageon, Thibault Tabarin, Yui Yamamoto, Yuanqing Ma, Philip R Nicovich, John S Bridgeman, André Cohnen, Carola Benzing, Yijun Gao, Michael D Crowther, et al. Functional role of t-cell receptor nanoclusters in signal initiation and antigen discrimination. *Proceedings of the National Academy of Sciences*, 113(37):E5454–E5463, 2016.
29. Sana Siddig, Sarah Aufmkolk, Sören Doose, Marie-Lise Jobin, Christian Werner, Markus Sauer, and Davide Calebiro. Super-resolution imaging reveals the nanoscale organization of metabotropic glutamate receptors at presynaptic active zones. *Science Advances*, 6(16): eaay7193, 2020.
30. Christian Sieben, Erdinc Sezgin, Christian Eggeling, and Suliana Manley. Influenza a viruses use multivalent sialic acid clusters for cell binding and receptor activation. *PLoS pathogens*, 16(7):e1008656, 2020.

31. Tomáš Lukeš, Daniela Glatzová, Zuzana Kvíčalová, Florian Levet, Aleš Benda, Sebastian Letschert, Markus Sauer, Tomáš Brdička, Theo Lasser, and Marek Cebecauer. Quantifying protein densities on cell membranes using super-resolution optical fluctuation imaging. *Nature communications*, 8(1):1–7, 2017.
32. Shirsendu Ghosh, Vincenzo Di Bartolo, Liron Tubul, Eyal Shimoni, Elena Kartvelishvily, Tali Dadosh, Sara W Feigelson, Ronen Alon, Andres Alcover, and Gilad Haran. Erm-dependent assembly of t cell receptor signaling and co-stimulatory molecules on microvilli prior to activation. *Cell Reports*, 30(10):3434–3447, 2020.
33. Sammy Frey, Mark Marsh, S Günther, Annegret Pelchen-Matthews, Paul Stephens, Susan Ortlepp, and Toon Stegmann. Temperature dependence of cell-cell fusion induced by the envelope glycoprotein of human immunodeficiency virus type 1. *Journal of virology*, 69(3): 1462–1472, 1995.
34. Hamani I Henderson and Thomas J Hope. The temperature arrested intermediate of virus-cell fusion is a functional step in hiv infection. *Virology journal*, 3(1):36, 2006.
35. Ruben M Markosyan, Fredric S Cohen, and Grigory B Melikyan. Time-resolved imaging of hiv-1 env-mediated lipid and content mixing between a single virion and cell membrane. *Molecular biology of the cell*, 16(12):5502–5513, 2005.
36. Pedro M Pereira, David Albrecht, Siân Culley, Caron Jacobs, Mark Marsh, Jason Mercer, and Ricardo Henriques. Fix your membrane receptor imaging: actin cytoskeleton and cd4 membrane organization disruption by chemical fixation. *Frontiers in immunology*, 10:675, 2019.
37. Carol Pitcher, Stefan Honing, Anja Fingerhut, Katherine Bowers, and Mark Marsh. Cluster of differentiation antigen 4 (cd4) endocytosis and adaptor complex binding require activation of the cd4 endocytosis signal by serine phosphorylation. *Molecular biology of the cell*, 10 (3):677–691, 1999.
38. Annegret Pelchen-Matthews, Ian J Parsons, and Mark Marsh. Phorbol ester-induced down-regulation of cd4 is a multistep process involving dissociation from p56lck, increased association with clathrin-coated pits, and altered endosomal sorting. *The Journal of experimental medicine*, 178(4):1209–1222, 1993.
39. Annegret Pelchen-Matthews, Jane E Armes, Gareth Griffiths, and Mark Marsh. Differential endocytosis of cd4 in lymphocytic and nonlymphocytic cells. *The Journal of experimental medicine*, 173(3):575–587, 1991.
40. Benhur Lee, Matthew Sharron, Luis J Montaner, Drew Weissman, and Robert W Doms. Quantification of cd4, ccr5, and cxcr4 levels on lymphocyte subsets, dendritic cells, and differentially conditioned monocyte-derived macrophages. *Proceedings of the National Academy of Sciences*, 96(9):5215–5220, 1999.
41. Maolin Lu, Xiaochu Ma, Luis R Castillo-Menendez, Jason Gorman, Nirmin Alsahafi, Utz Ermel, Daniel S Terry, Michael Chambers, Dongjun Peng, Baoshan Zhang, et al. Associating hiv-1 envelope glycoprotein structures with states on the virus observed by smfret. *Nature*, 568(7752):415–419, 2019.
42. James Arthos, Claudia Cicala, Elena Martinelli, Katilyn Macleod, Donald Van Ryk, Danlan Wei, Zhen Xiao, Timothy D Veenstra, Thomas P Conrad, Richard A Lempicki, et al. Hiv-1 envelope protein binds to and signals through integrin α 4 β 7, the gut mucosal homing receptor for peripheral t cells. *Nature immunology*, 9(3):301–309, 2008.
43. Claudia Cicala, Elena Martinelli, Jonathan P McNally, Diana J Goode, Ravindra Gopaul, Joseph Hiatt, Katija Jelicic, Shyamasundaran Kottilil, Katilyn Macleod, Angeline O'Shea, et al. The integrin $\alpha 4\beta 7$ forms a complex with cell-surface cd4 and defines a t-cell subset that is highly susceptible to infection by hiv-1. *Proceedings of the National Academy of Sciences*, 106(49):20877–20882, 2009.
44. Andrew CS Saphire, Michael D Bobardt, Zhe Zhang, Guido David, and Philippe A Gallay. Syndecans serve as attachment receptors for human immunodeficiency virus type 1 on macrophages. *Journal of virology*, 75(19):9187–9200, 2001.
45. Teunis BH Geijtenbeek, Douglas S Kwon, Ruurd Torensma, Sandra J van Vliet, Gerard CF van Duijnhoven, Jeena Middel, Ine LMHA Cornelissen, Hans SLM Nottet, Vineet N Kewal-Ramani, Dan R Littman, et al. Dc-sign, a dendritic cell–specific hiv-1-binding protein that enhances trans-infection of t cells. *Cell*, 100(5):587–597, 2000.
46. Craig B Wilen, John C Tilton, and Robert W Doms. Hiv: cell binding and entry. *Cold Spring Harbor perspectives in medicine*, 2(8):a006866, 2012.
47. William R Gallaher, Judith M Ball, Robert F Garry, Mark C Griffin, and RONALD C MONTELARO. A general model for the transmembrane proteins of hiv and other retroviruses. *AIDS research and human retroviruses*, 5(4):431–440, 1989.
48. Marta Barrero-Villar, José Román Cabrero, Mónica Gordón-Alonso, Jonathan Barroso-González, Susana Álvarez-Losada, M Ángeles Muñoz-Fernández, Francisco Sánchez-Madrid, and Agustín Valenzuela-Fernández. Moesin is required for hiv-1-induced cd4-cxcr4 interaction, f-actin redistribution, membrane fusion and viral infection in lymphocytes. *Journal of cell science*, 122(1):103–113, 2009.
49. Sujatha Iyengar, James EK Hildreth, and David H Schwartz. Actin-dependent receptor colocalization required for human immunodeficiency virus entry into host cells. *Journal of virology*, 72(6):5251–5255, 1998.
50. Jakub Chojnacki, Thorsten Staudt, Bärbel Glass, Pit Bingen, Johann Engelhardt, Maria Anders, Jale Schneider, Barbara Müller, Stefan W Hell, and Hans-Georg Kräusslich. Maturation-dependent hiv-1 surface protein redistribution revealed by fluorescence nanoscopy. *Science*, 338(6106):524–528, 2012.
51. Dzung H Nguyen, Banabihari Giri, Gary Collins, and Dennis D Taub. Dynamic reorganization of chemokine receptors, cholesterol, lipid rafts, and adhesion molecules to sites of cd4 engagement. *Experimental cell research*, 304(2):559–569, 2005.
52. D Mazea, G Schatten, and W Sale. Adhension of cells to surfaces coated with polylysine. *J Cell Biol*, 66:198–200, 1975.
53. Jay T Groves and Michael L Dustin. Supported planar bilayers in studies on immune cell adhesion and communication. *Journal of immunological methods*, 278(1-2):19–32, 2003.
54. Ana Mafalda Santos, Aleks Ponjavic, Marco Fritzsche, Ricardo A Fernandes, Jorge Bernardino de la Serna, Martin J Wilcock, Falk Schneider, Iztok Urbančič, James McColl, Consuelo Anzilotti, et al. Capturing resting t cells: the perils of pll. *Nature immunology*, 19(3):203–205, 2018.
55. Anna Oszmiana, David J Williamson, Shaun-Paul Cordoba, David J Morgan, Philippa R Kennedy, Kevin Stacey, and Daniel M Davis. The size of activating and inhibitory killer ig-like receptor nanoclusters is controlled by the transmembrane sequence and affects signaling. *Cell reports*, 15(9):1957–1972, 2016.
56. Björn F Lillemeier, Janet R Pfeiffer, Zurab Surviladze, Bridget S Wilson, and Mark M Davis. Plasma membrane-associated proteins are clustered into islands attached to the cytoskeleton. *Proceedings of the National Academy of Sciences*, 103(50):18992–18997, 2006.
57. Sinem K Saka, Alf Honigmann, Christian Eggeling, Stefan W Hell, Thorsten Lang, and Silvio O Rizzoli. Multi-protein assemblies underlie the mesoscale organization of the plasma membrane. *Nature communications*, 5(1):1–14, 2014.
58. Takahiro K Fujiwara, Kokoro Iwasawa, Ziya Kalay, Taka A Tsunoyama, Yusuke Watanabe, Yasuhiro M Umemura, Hideji Murakoshi, Kenichi GN Suzuki, Yuri L Nemoto, Nobuhiro Morone, et al. Confined diffusion of transmembrane proteins and lipids induced by the same actin meshwork lining the plasma membrane. *Molecular biology of the cell*, 27(7):1101–1119, 2016.
59. Kristen Feher, James M Halstead, Jesse Goyette, and Katharina Gaus. Can single molecule localization microscopy detect nanoclusters in t cells? *Current opinion in chemical biology*, 51:130–137, 2019.
60. Lekha Patel, Dylan M Owen, and Edward AK Cohen. Blinking statistics and molecular counting in direct stochastic reconstruction microscopy (dstorm). *bioRxiv*, page 834572, 2019.
61. Yuh-Jiin I Jong, Steven K Harmon, and Karen L O'Malley. Gpcr signalling from within the cell. *British journal of pharmacology*, 175(21):4026–4035, 2018.
62. Alyson Yoder, Dongyang Yu, Li Dong, Subashini R Iyer, Xuehua Xu, Jeremy Kelly, Juan Liu, Weifeng Wang, Paul J Vorster, Liane Agulto, et al. Hiv envelope-cxcr4 signaling activates cofilin to overcome cortical actin restriction in resting cd4 t cells. *Cell*, 134(5):782–792, 2008.
63. Beata Turoňová, Mateusz Sikora, Christoph Schürmann, Wim JH Hagen, Sonja Welsch, Florian EC Blanc, Sören von Bülow, Michael Gecht, Katrin Bagola, Cindy Hörner, et al. In situ structural analysis of sars-cov-2 spike reveals flexibility mediated by three hinges. *Science*, 370(6513):203–208, 2020.
64. Mark B Lucera, Zach Fleissner, Caroline O Tabler, Daniela M Schlatzer, Zach Troyer, and John C Tilton. Hiv signaling through cd4 and ccr5 activates rho family gtpases that are required for optimal infection of primary cd4+ t cells. *Retrovirology*, 14(1):1–13, 2017.
65. Ali Amara, Aurore Vidy, Genevieve Boulla, Karine Mollier, Javier Garcia-Perez, Jose Alcamí, Cedric Blanpain, Marc Parmentier, Jean-Louis Virelizier, Pierre Charneau, et al. G protein-dependent ccr5 signaling is not required for efficient infection of primary t lymphocytes and macrophages by r5 human immunodeficiency virus type 1 isolates. *Journal of virology*, 77 (4):2550–2558, 2003.

Online Methods

Cell Culture. SupT1([VB] ATCC® CRL-1942TM) is a $CD4^+/CCR5^-$ cell line derived from a T-cell lymphoblastic lymphoma. SupT1-R5 is a stable $CCR5^+$ derivative of SupT1 provided by James A. Hoxie (University of Pennsylvania). Suspension cultures of SupT1 and SupT1-R5 were maintained in phenol red-free RPMI 1640 medium (Life Technologies, 32404-014) supplemented with 10% foetal bovine serum (FBS; Sigma-Aldrich, F9665), GlutaMAX Supplement (Life Technologies, 35050-038), 50 U/ml penicillin, and 50 µg/ml strepto-mycin at a density of 1x 10^5 – 1x10^6 cells/ml at 37°C with 5% CO_2. Human embryonic kidney (HEK) 293T cells (ATCC® CRL-3216™) were cultured in Dulbecco's Modified Eagle Medium (DMEM; Life Technologies, 31053-028) supplemented with 10% FBS, GlutaMAX Supplement, 50 U/ml penicillin, and 50 µg/ml streptomycin at 37°C with 5% CO_2. HeLa-TZM-bl cells were cultured in DMEM, supplemented with 10% FBS and 1% GlutaMAX Supplement at 37°C with 5% CO_2.

Antibody conjugation. The monoclonal antibody OKT4 (anti-CD4) (1) was conjugated with Alexa Fluor fluorophores using NHS-ester chemistry Lightning Link Kits (Innova Biosciences). Briefly, 10 µg IgG (1mg/ml in PBS) were mixed with 1µl of LL-Modifier reagent, before the addition of 2-3 molar equivalents of NHS ester-functionalised Alexa Fluor 568 or Alexa Fluor 647 (from 10mg/ml stocks in DMSO). The reaction mixture was incubated at room temperature (RT, 23°C) for 3-4 hours. Subsequently, 1 µl of LL-Quencher was added to terminate the reaction. Unreacted fluorophore was removed by diluting the reaction volume to 500 µl and centrifugation through 3 kDa MWCO Amicon Ultra centrifugal filter columns at 14,000 relative centrifugal force (RCF) for 15 minutes. This washing step was repeated three times. Protein concentrations was determined by spectrophotometric measurement of absorbance at 280 nm and 280 nm vs 568 nm, respectively. Antibody cell labelling specificity was confirmed by comparison of immunolabeling signals of $CD4^+$ (Jurkat and SupT1) and $CD4^-$ (HEK293T) cells by epifluorescence microscopy.

Phorbol ester stimulation. SupT1-R5 cells (1x10^4 cells per sample) were pelleted and resuspended in 20µl cold RPMI-1640 with 0.4% FBS and 6 µg/ml OKT4-Alexa Fluor 647. Cells were incubated on ice for 60 minutes before washing, which was carried out by making up the cell volume to 10 ml in cold RPMI with 5% FBS and centrifuging the cells at 300 RCF for 6 min at 4°C. The supernatants were carefully aspirated and the cells washed twice in 10 ml cold RPMI-1640 with 5% FBS, as described above. Cells were resuspended in 60 µl of cold RPMI-1640, with 5% FBS, and allowed to settle on Poly-L-lysine (PLL)-coated coverslips (100 µg/ml in ddH_2O, Sigma-Aldrich, P8920) at 4°C for 40 minutes. Treated samples were transferred to 37°C RPMI-1640 with 5% FBS, with or without 2 mg/ml Phorbol-12-myristate-13-acetate (PMA) or 4-α-Phorbol-12-myristate-13-acetate (4α-PMA) and incubated for 15 minutes at 37°C. Thereafter, cells were returned to cold RPMI-1640 for 1-5 minutes and fixed with cold 4% paraformaldehyde (PFA) for 10 minutes. Control samples were transferred directly to cold 4% PFA without warming. Samples in PFA were then warmed to 37°C over 20 minutes, washed five times in PBS and stored in PBS until mounting for imaging.

Virus preparation. HEK 293T cells were seeded at 2.25 x 10^6 cells per T75 culture flask to give <50% cell confluency the following day. 1.5 ml of OptiMEM was mixed with 15 µg of $HIV_{JR\text{-}CSF}$ proviral DNA and incubated at RT for 5 min, before gently mixing with 45 µl Fugene 6 equilibrated to RT. Subsequently, cell medium was replaced with 15 ml antibiotic-free DMEM containing 10% FBS, after which the transfection reaction mixture was added and the cells were incubated at 37°C with 5% CO_2. After 48 hrs, the culture medium was collected and centrifuged at 500 RCF for 10 min. The supernatant was transferred to Beckman ultracentrifuge tubes underlaid with a 5 ml cushion of sterile 20% sucrose in PBS. The tubes were topped up with complete media and the virus pelleted through the sucrose cushion by ultracentrifugation at 98,000 RCF for 2 hours at 4°C. The supernatant was carefully aspirated to preserve the viral pellet, which was then resuspended in DMEM, aliquoted and stored at - 80°C in liquid nitrogen.

Virus titration. HeLa-TZM-bl cells were seeded at 1x10^3 cells per well in a 96 well microtiter plate. After 12-18 hours, the cells were infected with HIV in a series of two-fold dilutions from 1 in 2 to 1 in 256 in a final volume of 400 µl. At 6 hours post-infection (hpi), 8 µg Q4120 was added to each well to prevent syncytia formation. Cells were washed in PBS at 36 hpi and fixed in 4% PFA for 30 minutes at RT, followed by incubation in 0.1% PFA overnight at 4°C. Cells were then washed three times with PBS at RT, quenched in 50 mM NH_4Cl for 10 minutes, blocked and permeabilised with PBS supplemented with 1% FBS and 0.1% Triton for 15 minutes at RT, and finally washed with 1% FBS in PBS. Cells were incubated with mouse antiserum to HIV-1 p24/p55 Gag (ARP432; NIBSC Centre for AIDS Reagents, South Mimms, UK) at 1:500 in PBS containing 1% FBS for 1 hour at RT, washed three times with 1% FBS/PBS and incubated with Alexa Fluor 488 Goat anti-mouse IgG -Alexa Fluor 488 (H+L; Life Technologies, A-11029) and DAPI for 20-30 mins. Cells were washed with PBS before imaging the plates using a Perkin Elmer Opera Phenix high-throughput plate reader with a 20x air objective. Images (9 per well) were analysed using Columbus Image Analysis software.

HIV binding. 1x10^4 SupT1 and SupT1-R5 were pre-incubated with OKT4-Alexa Fluor 647 (6 µg/ml) in a total volume of 20 µl for 15 min at RT. The cells were then cooled to 4°C; HIV was added at a multiplicity of infection (MOI)

of 30 infectious units per cell and the cells incubated at 4°C. After 1 hr, free virus was removed by diluting the cells in 10 ml cold RPMI-1640 and centrifugation at 500 rpm for 10 min. The cell pellets were resuspended in 300 µl RPMI-1640 and allowed to settle onto PLL-coated µ-Slide 8 Well dishes (Ibidi GmbH, Gräfelfing, Germany) for 40 min. Settled cells were either fixed directly by incubation with 4% PFA in PBS for 30 minutes at RT (control sample), or the cold media was replaced with pre-warmed media, and samples incubated at 37°C for 1 minute before fixing as described above. After fixation, samples were washed three times with PBS and permeabilised in 0.1% Tween-20 in PBS for 5 minutes, blocked for 20 min in PBS containing 4% BSA, and labelled with anti-HIV Gag antiserum as above. The cells were then washed three times in PBS and incubated with 1:500 Goat-anti-mouse-Alexa Fluor 568 (Life Technologies, A-11004) for 1 hour at RT, then washed five times in PBS (5min for each wash), subjected to a second round of fixation with 4% PFA in PBS for 30 minutes at RT, washed five times in PBS and stored in PBS before mounting for analysis by microscopy.

gp120 binding. SupT1 and SupT1-R5 cells ($1x10^4$ cells per sample) were pelleted and resuspended in 20µl cold RPMI-1640 with 0.4% FBS and 6 µg/ml OKT4-Alexa Fluor 647, with or without 1 µg/ml HIV_{Bal} gp120 (NIH AIDS Reagents Program). Cells were incubated on ice for 60 minutes before being diluted in 10 ml cold RPMI-1640 containing 5% FBS and centrifuging at 300 RCF for 6 min at 4°C. The supernatants were carefully aspirated, and the cells resuspended and washed twice in 10 ml cold RPMI-1640 containing 5% FBS. The cells were then resuspended in 60 µl cold RPMI-1640 containing 5% FBS and allowed to settle on PLL-coated coverslips (100 µg/ml in ddH_2O, Sigma-Aldrich, P8920), on ice, for 40 minutes. Control samples were transferred directly to cold 4% PFA. Treated samples were transferred to 37°C RPMI-1640 containing 5% FBS for 1 minute, before returning to cold RPMI-1640 for 5 minutes. The cells were then fixed with cold 4% PFA for 10 minutes, before warming to 37°C over 20 minutes. Samples were washed five times in PBS and stored in PBS until mounting for imaging.

Imaging. Samples prepared on coverslips were mounted on parafilm-formed gaskets (as described in (2)) with STORM buffer (150 mM Tris pH 8, 1% glycerol, 1% glucose, 10mM NaCl, 1% beta-mercaptoethanol, 0.5 mg/ml glucose oxidase, and 40 µg/ml catalase) and sealed with clear nail varnish. For samples on Ibidi GmbH slides, the sample wells were filled with STORM buffer, and the lid sealed with High- Performance Black Masking Tape (Thorlabs, UK).

Imaging was carried out on a Zeiss Elyra PS.1, with an alpha Plan-Apochromat DIC M27 Elyra 100x 1.46 Numerical Aperture (NA) oil objective, additional 1.6x optovar magnification, and Andor iXon 897 electron multiplication CCD (EMCCD) camera, yielding a pixel size of 100 nm. STORM datasets of 15,000 sequential frames were acquired in Total internal reflection fluorescence (TIRF) configuration, using 33 ms exposure time, with 642 nm or 561 nm excitation at maximum power output (approx.3.98 kW/cm^2 and 3.71 kW/cm^2 on the sample, respectively). Fluorophore photoswitching was dynamically controlled using periodic 405 nm illumination at the intensity of approx. 0 – 0.0586 kW/cm^2 on sample laser power. EM camera gain of 300 was used. Microscope autofocus was used throughout all acquisitions.

Localisation algorithm. SMLM imaging datasets were processed using the ThunderSTORM analysis plugin (3). Initial particle localisation was performed using the local maximum method, followed by sub-pixel localisation using the integrated Gaussian model and fitting by Maximal Likelihood Estimation. Drift correction was performed post-localisation by cross-correlation (number of bins was 5.0). Reconstructed images were rendered using a normalised 20 nm Gaussian.

Cluster analysis. For cluster analysis, we used Clus-DoC (4). 30nm Epsilon and 1 Minimum point parameters were used throughout the study. We manually selected our regions of interests (ROIs) to include as much of the plasma membrane as possible while but avoiding cell-edge effects. For each cluster, we obtained the area and corresponding mean diameter, the cluster density per ROI (number of clusters detected/ROI area [μm^2]) as well as the number of localisations for each cluster.

Cluster manual annotation. To validate the quantitative results from Clus-DoC (4), we manually annotated clusters in Fiji (5); cross-sections of identified clusters were drawn individually. The intensity profile was plotted and fitted with a Gaussian distribution of standard deviation σ. The cluster diameter was estimated using the Full-Width Half Maximum (FWHM) as $d=2.35\sigma$.

Channel registration. Channel registration was performed using a chromatic aberration correction plugin developed by the Jalink lab (https://jalink-lab.github.io/). Fiducial bead-coated coverslips were imaged for each experiment under both 647 nm and 568 nm channels. Fiducial bead images were used as references for estimating the transformation between channels. This correction was directly measured and applied to localisation data.

Colocalisation analysis. To determine the colocalisation threshold, we used post-channel registration fiducial bead images. When the optimised threshold was set to 0.4, the majority of events co-localised (>99%) with a peak of the DoC distribution at 1, indicating high colocalisation. Aside from the DoC score, we also extracted information on the percentage of colocalisation between channels and the mean cluster diameter in the colocalised and non-colocalised areas.

Molecular counting. We performed molecular counting as described (6). To calibrate the grouping parameters, we performed the same STORM imaging procedure as described in **Localisation algorithm** on isolated conjugated antibodies. The imaging dishes were incubated with 1 µg/ml dye-conjugated CD4 antibody for 15min. The dishes were washed once and then imaged under the same experimental conditions as for the main dataset using T cells. Images were reconstructed as described in **Cluster analysis**. Localisations within 30nm were merged as one lo-calisation frame by frame to form a new coordinates map and temporally binned to extract calibration parameters for molecular counting. All localisation processing was performed using custom-written MATLAB (MathWorks) scripts (kindly provided by Christian Sieben).

Theoretical Poisson statistical model. We used a theoretical model based on cluster-size specific Poisson probability distributions to determine whether our results for CD4 molecule numbers in clusters are consistent with a random distribution of receptors on the cell surface.

We generated theoretical distributions of the number of molecules per cluster expected for a random distribution of receptors using an average CD4 surface density n = 200 molecules/µm^2. This comes from considering a CD4 density of 100,000 molecules/cell in SupT1-R5 cells (7, 8) and typical T-cell shapes with a radius of 10 µm. Cells were approximated as a flat disk with total surface area $2\times\pi r^2 = 630$ μ^2. The expected probability of observing a number of receptors k in a given area A of the cell surface is given by the discrete Poisson probability distribution, P(k; λ), where k>=0 and λ=nA is the mean receptor count expected when counting receptors on a patch of area A (λ is also the mean of the distribution). This simple model assumes independence of receptor-counting events and, hence, no interactions between receptors, signalling or active processes or receptor mobility are considered. Thus, in this model, counting of multiple CD4 receptors in a given area is considered to be purely due to chance, i.e. to random statistical fluctuations.

Our imaged CD4 clusters had radii (r_i) in the range 10-100 nm (considering their equivalent circular areas). Their corresponding mean parameters (λ_i) are therefore in the range 0.1-6. The Poisson distribution has significantly different shapes for these different values of its mean parameter, and is increasingly asymmetrical for decreasing values of λ_i below 5. For the larger cluster sizes (larger λ_i), the distribution mean (and peak position) shifts to higher values of k and the probability of counting a larger number of molecules per cluster increases. For these reasons, our model considered the different sizes of all the measured clusters to calculate the overall probability distribution of numbers of molecules per cluster that would be observed when counting receptor numbers in circular cluster areas equivalent to those occupied in our measured CD4 clusters.

The expected overall distribution of numbers of molecules per cluster is therefore the average of the Poisson distributions corresponding to all our observed cluster sizes (areas of radius r_i). The overall probability (P) of counting k receptors is:

$$p(k) = \frac{1}{N}\sum_{i=1}^{N} p(k;\lambda_i) \qquad \textbf{(1)}$$

where we summed over all the different clusters (i is the cluster index and N is the total number of clusters measured), $P(k;\lambda_i)$ is the Poisson distribution for a given cluster i with radius r_i (that occupies a surface area $A_i=\pi r^2_i$, and $\lambda_i=nA_i=\pi r^2_i n$ is the corresponding mean value of the Poisson distribution for cluster i In order to compare expected and measured distributions, we re-normalised our expected distributions by excluding k=0 and dividing by the sum of the remaining counts. This is because areas with zero receptors were not measured in our experiments. Calculations were performed using custom-written Python scripts.

Statistical analysis. All data are presented as means ± standard deviation (SD) from three independent experiments. N is indicated in each figure separately. Student t-tests were performed by GraphPad Prism 8 (Prism Software). Significance was calculated using unpaired Student's t tests.

Bibliography

1. Ellis L Reinherz, Patrick C Kung, Gideon Goldstein, and Stuart F Schlossman. Separation of functional subsets of human t cells by a monoclonal antibody. *Proceedings of the National Academy of Sciences*, 76(8):4061–4065, 1979.
2. Pedro M Pereira, David Albrecht, Siân Culley, Caron Jacobs, Mark Marsh, Jason Mercer, and Ricardo Henriques. Fix your membrane receptor imaging: actin cytoskeleton and cd4 membrane organization disruption by chemical fixation. *Frontiers in immunology*, 10:675, 2019.
3. M Ovesnỳ. Kr ı z ek, p., borkovec, j., s vindrych, z. and hagen, gm(2014). thunderstorm: a comprehensive imagej plug-in for palm and storm data analysis and super-resolution imaging. *Bioinformatics*, 30:2389–2390.
4. Sophie V Pageon, Philip R Nicovich, Mahdie Mollazade, Thibault Tabarin, and Katharina Gaus. Clus-doc: a combined cluster detection and colocalization analysis for single-molecule localization microscopy data. *Molecular biology of the cell*, 27(22):3627–3636, 2016.
5. Johannes Schindelin, Ignacio Arganda-Carreras, Erwin Frise, Verena Kaynig, Mark Longair, Tobias Pietzsch, Stephan Preibisch, Curtis Rueden, Stephan Saalfeld, Benjamin Schmid, et al. Fiji: an open-source platform for biological-image analysis. *Nature methods*, 9(7): 676–682, 2012.
6. Christian Sieben, Erdinc Sezgin, Christian Eggeling, and Suliana Manley. Influenza a viruses use multivalent sialic acid clusters for cell binding and receptor activation. *PLoS pathogens*, 16(7):e1008656, 2020.
7. Annegret Pelchen-Matthews, Jane E Armes, Gareth Griffiths, and Mark Marsh. Differential endocytosis of cd4 in lymphocytic and nonlymphocytic cells. *The Journal of experimental medicine*, 173(3):575–587, 1991.
8. Benhur Lee, Matthew Sharron, Luis J Montaner, Drew Weissman, and Robert W Doms. Quantification of cd4, ccr5, and cxcr4 levels on lymphocyte subsets, dendritic cells, and differentially conditioned monocyte-derived macrophages. *Proceedings of the National Academy of Sciences*, 96(9):5215–5220, 1999.

Supplementary Figures

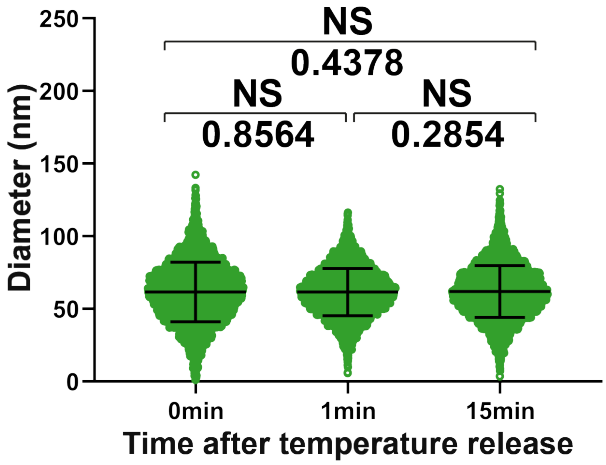

Fig. S1. Quantification of CD4 cluster diameters at different time points after releasing the temperature block. Each dot represents 1 cluster. 15 cells were imaged per condition with the mean cluster diameter ± SD indicated by the black bar. A total of 8123, 7822 and 7932 clusters were detected, respectively. The data are representative of at least three independent experiments.

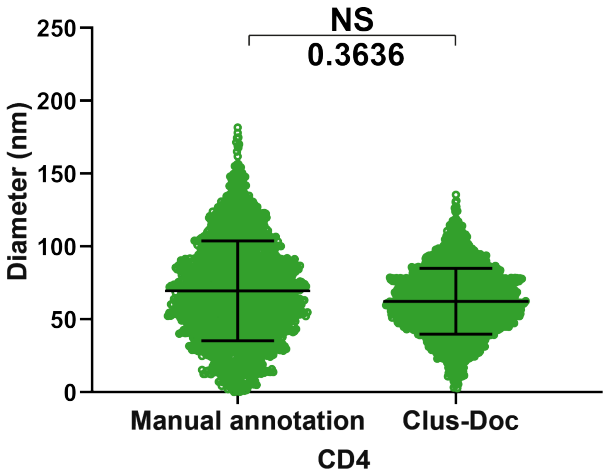

Fig. S2. Comparison of CD4 cluster diameters distributions between automated Clus-DoC analysis and manual measurements. Each dot represents 1 cluster. 10 cells were measured per condition with the mean cluster diameter ± SD indicated by the black bar. The total number of clusters detected in the manual annotation and DoC were 9731 and 7892, respectively. The data are representative of at least three independent experiments.

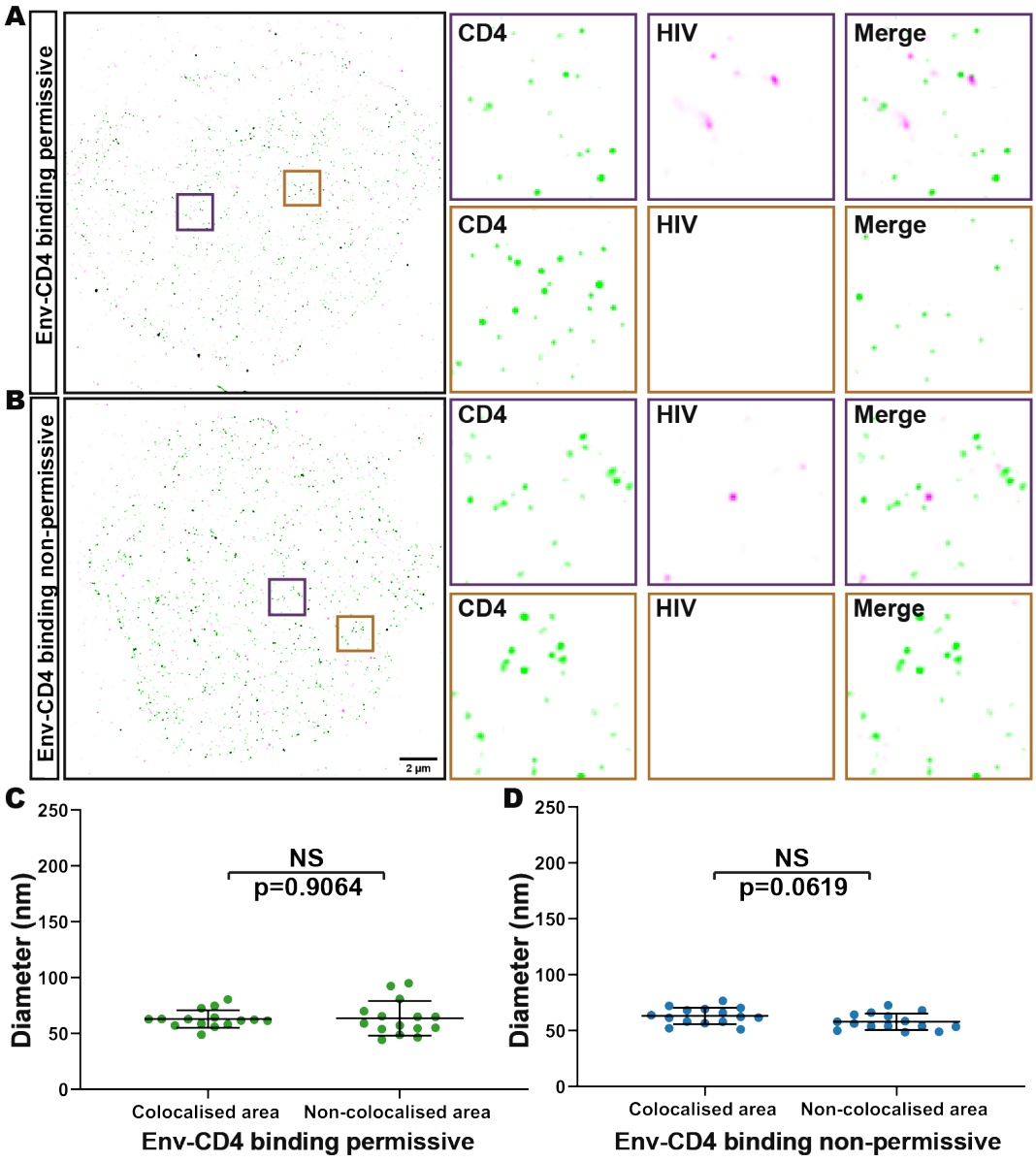

Fig. S3. CD4 does not cluster on HIV-1 treated cells and untreated cells kept at 4℃ A. and B. Representative STORM images of CD4 clusters on cells fixed directly without release temperature block. HIV-1 was labelled with anti-p24 and anti-mouse Ig-Alexa Fluor 568. Scale bar = 2 µm. **C. and D.** Quantification of CD4 cluster diameters in the absence (Env-CD4 binding permissive) and presence (Env-CD4 binding non-permissive) of Q4120. In Env-CD4 binding inhibition group, SupT1-R5 cells were pre-incubated with Q4120 (an anti-CD4 antibody that inhibits HIV gp120-CD4 binding). Each dot represents the average diameter of CD4 clusters for one cell. 15 cells were measured per condition with the mean ± SD indicated by the black bar. The data are representative of at least three independent experiments. * $p< 0.05$; ** $p< 0.01$; *** $p< 0.001$; **** $p< 0.0001$.

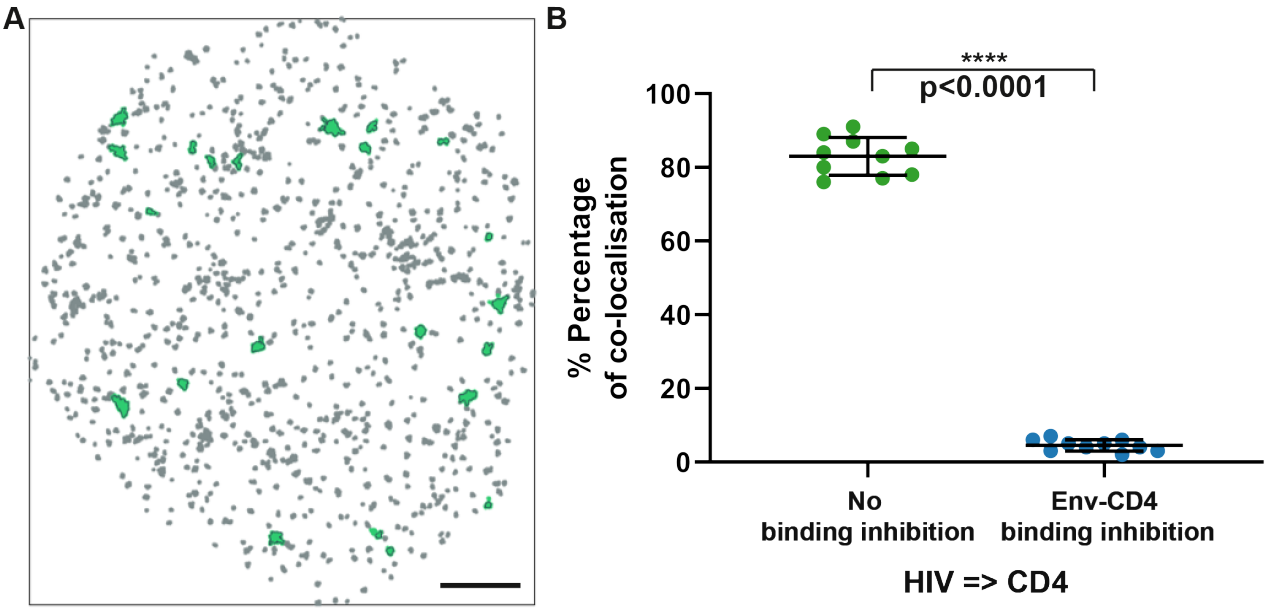

Fig. S4. Analysis of the percentage of CD4 clusters colocalised with HIV p24 signal.A. Representative image tracing enlarged CD4 clusters that colocalised with HIV p24 signal on the same cell illustrated in Figure 3B. **B.** The percentage of HIV particles colocalised to CD4 in the 'Permissive' and 'Non-permissive' as obtained from Clus-DoC co-clustering analysis. Each data point represents a cell. The data are from ten different cells in three separate experiments. * p< 0.05; ** p< 0.01; *** p< 0.001; **** p< 0.0001.

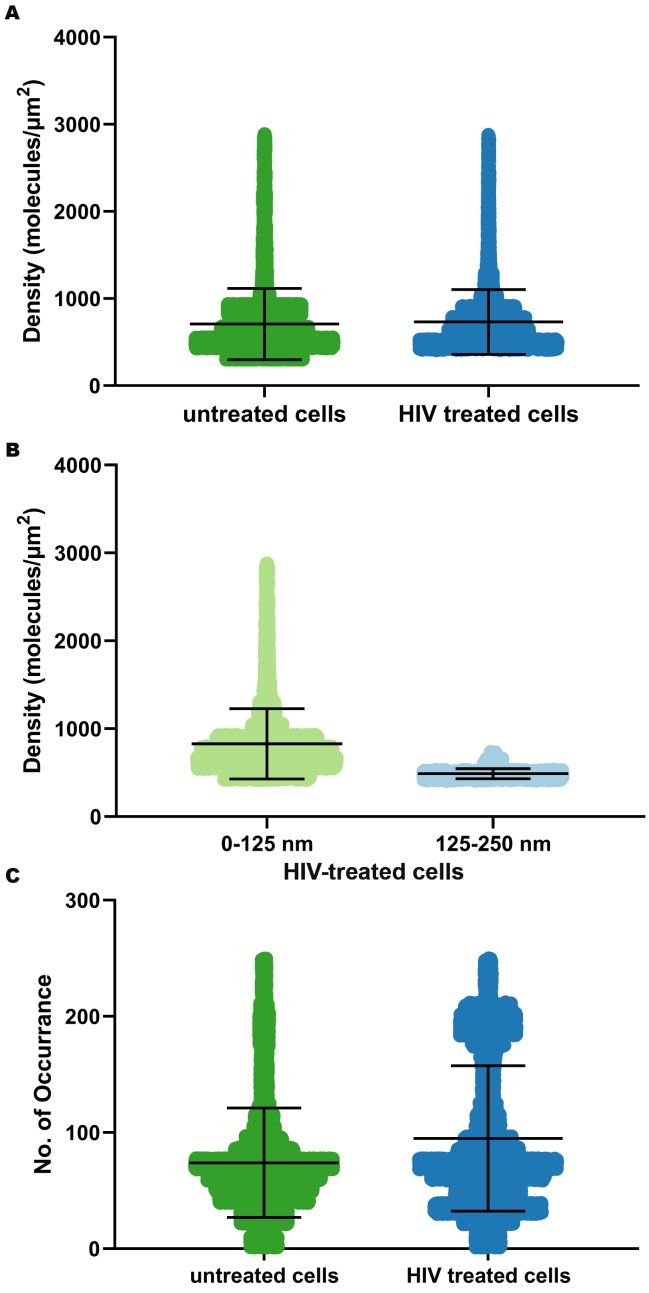

Fig. S5. Diameters and densities of CD4 clusters on HIV-treated cells and untreated cells. A. Distribution of CD4 molecule density of CD4 molecules on untreated cells and HIV-treated cells. Data from 15 cells were plotted. **B.** Distribution of CD4 molecule density for cluster diameter 0-125 nm and 125-250 nm on HIV treated cells. **C.** Distributions of CD4 cluster diameters on untreated cells and HIV-treated cells. Each point represents 1 cluster; Bars represent mean ± SD.

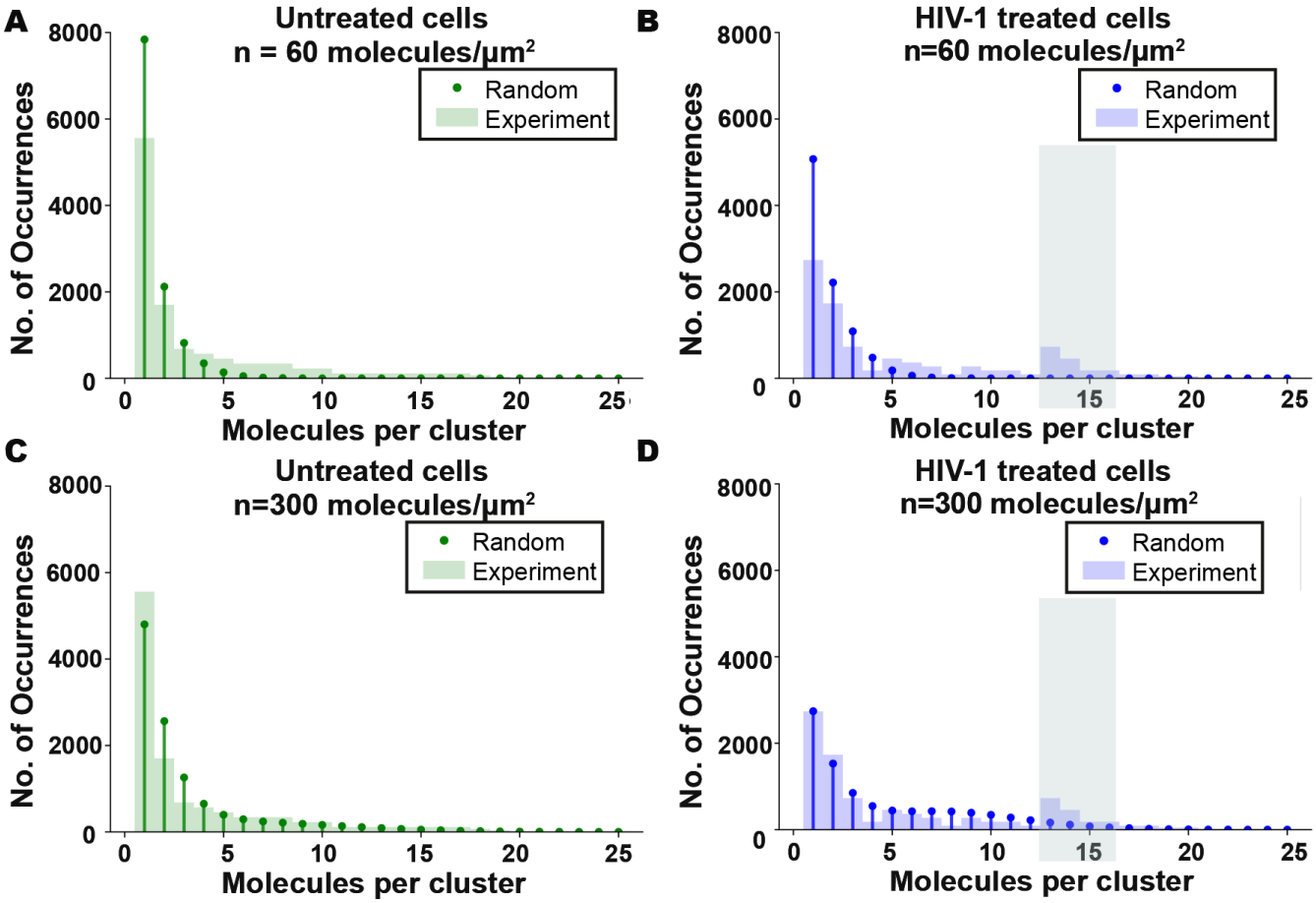

Fig. S6. Statistical modelling of CD4 surface distribution using different molecule density in the model. Comparison of expected and measured distributions of numbers of molecules per cluster for untreated cells **(A, C)** and HIV-treated cells **(B, D)**. **A. and B.** represents Poisson distribution data from lower mean density (n=60 molecules/μm^2) than showed in Figure 4 (n=200 molecules/μm^2). **C. and D.** were Poisson distribution data from higher density (n=300 molecules/μm^2) than showed in Figure 4 (n=200 molecules/μm^2). The discrepancy between predicted model and experimental data in HIV-treated cells is highlighted in green shading in **B** and **D**. Data from at least three separate experiments and 15 different cells in each condition, respectively.